Nanoscale Advances

PAPER

View Article Online
View Journal | View Issue

Cite this: *Nanoscale Adv.*, 2019, **1**, 4109

PbS quantum dots as additives in methylammonium halide perovskite solar cells: the effect of quantum dot capping†

Thi Tuyen Ngo,[a] Sofia Masi,[a] Perla F. Mendez,[ab] Miri Kazes,[c] Dan Oron[c] and Iván Mora Seró*[a]

Colloidal PbS quantum dots (QDs) have been successfully employed as additives in halide perovskite solar cells (PSCs) acting as nucleation centers in the perovskite crystallization process. For this strategy, the surface functionalization of the QDs, controlled *via* the use of different capping ligands, is likely of key importance. In this work, we examine the influence of the PbS QD capping on the photovoltaic performance of methylammonium lead iodide PSCs. We test PSCs fabricated with PbS QD additives with different capping ligands including methylammonium lead iodide (MAPI), cesium lead iodide (CsPI) and 4-aminobenzoic acid (ABA). Both the presence of PbS QDs and the specific capping used have a significant effect on the properties of the deposited perovskite layer, which affects, in turn, the photovoltaic performance. For all capping ligands used, the inclusion of PbS QDs leads to the formation of perovskite films with larger grain size, improving, in addition, the crystalline preferential orientation and the crystallinity. Yet, differences between the capping agents were observed. The use of QDs with ABA capping had a higher impact on the morphological properties while the employment of the CsPI ligand was more effective in improving the optical properties of the perovskite films. Taking advantage of the improved properties, PSCs based on the perovskite films with embedded PbS QDs exhibit an enhanced photovoltaic performance, showing the highest increase with ABA capping. Moreover, bulk recombination *via* trap states is reduced when the ABA ligand is used for capping of the PbS QD additives in the perovskite film. We demonstrate how surface chemistry engineering of PbS QD additives in solution-processed perovskite films opens a new approach towards the design of high quality materials, paving the way to improved optoelectronic properties and more efficient photovoltaic devices.

Received 2nd August 2019
Accepted 10th September 2019

DOI: 10.1039/c9na00475k

rsc.li/nanoscale-advances

1. Introduction

Lead halide perovskites (HPs) have attracted worldwide attention, predominantly due to the rapid progress in HP-based photovoltaics. The certified photoconversion efficiency (PCE) of halide perovskite solar cells (PSCs) has reached over 25% [1] in 2019, a staggering improvement on the already remarkable breakthrough in 2012 with PCEs of around 10%, first reported for all-solid PSCs.[2,3] The unprecedented quick progress in PCE of PSCs has been mainly attributed to the superb optoelectronic properties of HP materials such as high absorption coefficient and long carrier diffusion lengths.[4,5] Besides, HPs have also been demonstrated as promising materials for light emitting diodes (LEDs),[6–8] photodetectors,[9] light amplifiers[10,11] and lasers.[12–14]

A variety of approaches have been employed in the optimization process of PSCs, including the use of different device configurations[2,15] and different HP materials.[16] The quality of the HP layer has also been improved in various ways including solvent,[17] compositional[18,19] and interface engineering.[20,21] Solution deposition techniques have been extensively used in the fabrication of PSCs. These solution methods also allow the easy combination of HPs with other materials, such as organic molecules,[22–24] polymers,[25–29] or colloidal quantum dots (QDs).[30,31] The interaction between HPs and QDs can lead to interesting synergistic properties.[32,33] In particular, the combination of PbS QDs and methylammonium lead iodide (MAPI) has been studied as both materials possess six-coordinated Pb atoms with similar Pb–Pb distances (6.26 Å for MAPI and 5.97 Å for PbS) and less than 4.6% lattice mismatch.[31] One recent report showed that with an appropriate amount of organically capped PbS QDs (mixture of oleic acid, oleylamine and trioctylphosphine), the properties of HP film including morphological, optical and structural properties can be improved, increasing the PCE of PSCs from 16.3% for

[a]*Institute of Advanced Materials (INAM), Jaume I University, 12006 Castellón, Spain. E-mail: sero@uji.es*

[b]*Facultad de Ciencias Químico Biológicas, Universidad Autónoma de Sinaloa, Cd. Universitaria, Av. de las Américas y Josefa Ortiz S/N, 80000, Culiacán, Sinaloa, Mexico*

[c]*Department of Physics of Complex Systems, Weizmann Institute of Science, Rehovot 76100, Israel*

† Electronic supplementary information (ESI) available. See DOI: 10.1039/c9na00475k

pure MAPI to 18.6% for hybrid HP–QD absorbers.[34] We showed that the interaction between HPs and PbS/CdS QDs capped with the MAPI ligand gives rise to a new light emission peak (either as photoluminescence or as electroluminescence) from an exciplex state at a lower bandgap than both HPs and PbS/CdS QDs.[30] Moreover, a positive effect of embedded QDs on HP morphology, with an increase of grain size, was also observed.[30,34,35] These studies demonstrated that a small amount of PbS QDs dispersed in the HP precursor solution can serve as effective seed-like nucleation centers, resulting in a better HP layer quality and improved optoelectronic properties.[34,35] A similar effect on perovskite properties was also observed for the case of intermixing SnS QDs, capped with triethanolamine, with a MAPI perovskite, although the lattice mismatch between SnS and MAPI is higher.[36]

In QD solar cells, the QD capping has a clear impact on the device performance.[37–39] Recently, HP precursors such as MAI[40] and lead mixed halides (PbI_2 + $PbBr_2$)[41] and HPs, such as MAPI [42] and CsPI,[43] have been used as the ligands of PbS QDs. The PCE of PbS QD solar cells has been improved, reaching over 11% for the lead mixed halide capping.[41] In addition, improvement of HP properties by QD incorporation was observed with several types of capping ligands, including organic molecules,[34,36] and HP precursors (MAI[35] and MAPI).[30] The question of how the choice of ligand can also be exploited as a control mechanism for the structural and optoelectronic properties of HP and in turn the efficiency of the QD-containing PSCs is, nevertheless, still open.

In this work, ligands of the as-synthesized PbS QDs with an oleate (OA) capping were exchanged with three different ligands: MAPI, cesium lead iodide (CsPI) and 4-aminobenzoic acid (ABA), and then separately dispersed in a solution containing HP precursors (PbI_2 and MAI) at different concentrations. Hybrid HP–PbS QD films were prepared *via* a one-step spin-coating method.[30] With a small amount of embedded PbS QDs, we observed an increase in HP grain sizes, reduction in non-radiative recombination, better preferential orientation and increased crystallinity of HPs for all three different ligands, with a more prominent effect for the ABA capping. Hybrid methylammonium lead iodide–PbS (HP–PbS) QD films have been used in the fabrication of planar PSCs with SnO_2 as the electron selective layer. This is a very promising configuration for commercialization of PSCs as SnO_2 [21] does not require high temperature treatments and the planar architecture presents advantages in terms of cost and environmental impact as compared with cells containing a mesoporous layer.[44] We observed that the use of small concentrations of PbS QDs in planar SnO_2/HP-PbS/spiro-OMeTAD perovskite solar cells showed an increase in the PCE relative to reference cells without PbS QDs. More importantly, this had a significant beneficial effect on cell PCE, where the highest increase in PCE was obtained for ABA capping, with the champion cell exhibiting a PCE of 16.6%.

2. Experimental section

2.1. Synthesis of PbS QDs

PbS QDs were synthesized according to a previously reported procedure with some modifications.[30] Briefly, a three-neck round-bottom flask containing PbO (0.9 g), oleic acid (OA, 2.7 g) and 1-octadecene (ODE, 36 ml) was heated at 120 °C under vacuum for 90 minutes. The temperature was raised to 150 °C for 15 minutes to form Pb-oleate. Next, N_2 was introduced to the system and 3 ml of trioctylphosphine (90%) were injected. Subsequently, the temperature was reduced to 110 °C. Then, a mixture of 0.42 ml hexamethyldisilathiane (HMDS) and 4 ml ODE was quickly injected into the flask. The temperature was then gradually decreased to room temperature. The reaction product was cleaned 3 times with ethanol/acetone (1 : 1, v/v), centrifuged (3000 rpm for 10 minutes) and dispersed in octane (10 mg ml^{-1}). The photoluminescence (PL) and absorbance of the as-synthesized PbS QDs are presented in Fig. S1.† The size of PbS QDs was estimated to be ~3.5 nm, according to the literature[45]

$$E_o = 0.41 + \frac{1}{0.0252d^2 + 0.283d}$$

where d is the diameter of PbS QDs and E_o is the energy of emitted photons at the peak of the PL spectrum.

2.2. PbS ligand exchange

Exchange with the methylammonium lead iodide (MAPI) ligand. The PbS ligand exchange of oleate (OA) with MAPI was performed following a previously reported procedure[30] with a small modification. 115 mg of PbI_2 and 40 mg of CH_3NH_3I (MAI) were dispersed in 1 ml of dimethylformamide (DMF), forming 0.25 M MAPI solution. Then, 0.5 ml of QDs dispersed in octane (10 mg ml^{-1}) was added into 0.5 ml of 0.25 M MAPI solution. After stirring for 30 minutes, QDs had transferred from the top octane phase to the bottom DMF. After removing the octane, the QD solution was washed three more times using octane to remove the organic residue. Subsequently, the QDs were precipitated by the addition of toluene, and then centrifuged at 3500 rpm for 5 minutes. After removing all the liquid, QDs were dried under vacuum for several hours.

Exchange with the cesium lead iodine (CsPI) ligand. The process for the exchange of the oleate (OA) with the CsPI ligand was identical to that for the exchange with MAPI; however, 65 mg of CsI was used instead.

Exchange with the 4-aminobenzoic acid (ABA) ligand. 1 ml of 0.05 M ABA in DMF was diluted with 1 ml of absolute ethanol. Then 2 ml of PbS_OA QDs (2.5 mg ml^{-1} in octane) were added into the ABA solution. Similar to the case of the exchange with MAPI or CsPI, after mixing ABA and PbS solutions and shaking the mixture for a few minutes, as a result of which phase transfer took place, the QDs had transferred to DMF, leading to a color change of the bottom phase from transparent to dark, and the opposite for the top phase (dark to transparent). PbS QDs were cleaned, precipitated, centrifuged and dried as described above. During the ligand exchange, PbS QDs were protected from light as much as possible.

To simplify, PbS QDs exchanged with MAPI, CsPI and ABA are hereafter termed PbS_MAPI, PbS_CsPI and PbS_ABA, respectively.

2.3. SnO_2 compact layer

FTO substrates were cleaned with soap, sonicated in distilled water, ethanol and isopropanol for 15 minutes and then treated

with a UV (ultraviolet)-O_3 lamp for 15 minutes. The SnO_2 compact layer was prepared according to a previous report[46] with a small variation. 296 μl of commercial SnO_2 solution (tin(IV) oxide, 15% in H_2O colloidal dispersion from Alfa Aesar) was diluted with 1.71 ml of ultrapure water. Then, 100 μl of this diluted SnO_2 solution was poured on an FTO substrate and spin-coated at 3000 rpm (acceleration of 3000 rpm) for 40 seconds. SnO_2 films were annealed at 150 °C for 30 minutes.

2.4. Perovskite (HP) and HP–PbS solution and film preparation

1.33 M MAPI solution was prepared by dissolving 612 mg of PbI_2 and 211 mg of MAI in dimethyl sulfoxide (DMSO) at 70 °C. Dried PbS QDs with different ligands were separately dispersed in 0.4 ml of 1.33 M MAPI solution. The amount of PbS QDs introduced in the ligand exchange was 5 mg for each exchange and we assumed that there was no loss of PbS QDs during the ligand exchange. Therefore, their concentration in 0.4 ml of MAPI solution was considered to be 12.5 mg ml^{-1}, which was used as the mother solution. The HP–PbS mother solutions were further diluted with 1.33 M MAPI solution to a weight concentration of PbS QDs of 50 and 100 μg ml^{-1}. The MAPI and MAPI-PbS films were prepared by spin-coating 1.33 M MAPI solution without and with PbS QDs at 2000 rpm for 10 seconds (acceleration of 200 rpm) and then at 6000 rpm for 30 seconds (acceleration of 2000 rpm). After 25 seconds of spinning, ethyl acetate was poured on the films. MAPI and MAPI-PbS films were annealed at 130 °C for 10 minutes. All solution and film depositions were performed inside a glovebox filled with N_2.

2.5. Spiro-OMeTAD and gold

Spiro-OMeTAD solution was prepared by dissolving 72.3 mg of spiro-OMeTAD (2,2′,7,7′-tetrakis(*N*,*N*-di-*p*-methoxyphenylamine)-9,9-spirobifluorene) in 1 ml of chlorobenzene, and then mixing it with 28.8 μl of 4-*tert*-butylpyridine and 17.5 μl of a stock Li^+ solution (which contained 520 mg ml^{-1} bis-trifluoromethylsulfonylamine lithium salt in acetonitrile). The spiro-OMeTAD layer was spin-coated on HP or HP–QD films at 4000 rpm for 30 seconds (acceleration of 800 rpm). Finally, 80 nm of gold was thermally evaporated in an ultrahigh vacuum chamber on top of the spiro-OMeTAD layer to make complete devices.

2.6. Sample preparation for Fourier-transform infrared (FT-IR) measurement

ABA was dispersed in DMSO (38 mg ml^{-1}). PbS_OA QDs were exchanged with the ABA capping ligand following the procedure listed above. After ligand exchange, PbS_ABA QDs were dried and dissolved in 0.6 ml of 1.33 M perovskite precursors (PbI_2 and MAI).

2.7. Characterization of samples in solution and film

The morphology of the films was analyzed by scanning electron microscopy (SEM) using a JSM7001F (field emission scanning electron microscope). The absorbance spectrum of the as-synthesized PbS QDs (with the oleate ligand, PbS_OA) was measured using a Cary 500 Scan Varian UV-VIS-NIR spectrophotometer. The photoluminescence (PL) measurement of PbS_OA, PbS_MAPI, and PbS_CsPI QDs in solution was carried out using a CCD detector (InGaAs Andor-iDUS DU490A-2.2) coupled with an adaptive focus imaging spectrograph (Kymera KY-193i-B2). A commercial continuous laser (532 nm, GL532RM-150) was used as an excitation source. The PL spectra of PbS_ABA QDs in solution were measured using a Fluorolog system (Horiba Jobin Yvon) with a 532 nm excitation wavelength. PL spectra of MAPI and MAPI-PbS films were also measured using the same Fluorolog system and excitation. For the PL measurement, a long-pass filter, 20CGA-590, was used in order to block the excitation source. A Bruker AXS-D4 Endeavor Advance X-ray diffractometer with Cu Kα radiation was used to measure the X-ray diffraction (XRD) spectra of MAPI and hybrid HP–PbS films. Fourier-transform infrared absorption (FT-IR) was measured using an FT-IR 6200 spectrometer (Jasco) with an ATR Pro One (Jasco) equipped with a diamond crystal.

2.8. Device characterization

Photocurrent density–voltage (*J–V*) characteristics. The *J–V* curves of solar cells were measured under a xenon arc lamp simulator equipped with an AM 1.5 spectral filter (solar simulator 69920, Newport). The intensity was adjusted to provide 1 sun (100 mW cm^{-2}) by using a calibrated silicon solar cell. The *J–V* characteristics were recorded by scanning the potential from higher than the open circuit voltage (V_{oc}) to −0.05 V (backward mode) at approximately 45 mV s^{-1}.

Incident photon to current efficiency (IPCE) measurements. The IPCE measurements were performed employing a 150 W xenon lamp coupled with a computer-controlled monochromator. The photocurrent was measured using an optical power meter (model 70310, Oriel Instruments). A Si photodiode was used to calibrate the system.

3. Results and discussion

The absorbance and PL spectra of the as-synthesized PbS QDs used in this work, with OA ligands, are shown in Fig. S1.† As can be seen, the PL spectrum presents a fairly narrow peak, pointing to a relatively homogeneous distribution of QD sizes centered around a diameter of ∼3.5 nm (see the Experimental section). The OA ligands serve to control the size of QDs, to prevent their aggregation in the organic solution and to electronically passivate the QD surface. An important step to realize perovskite photovoltaic devices is exchanging these long chain ligands with short and polar ones, to favor the HP–PbS QD interaction and simultaneously make them soluble in DMF and DMSO, which are commonly employed to dissolve the HP precursors. This process allows us to overcome the solubility limitation, and to develop a one-step deposition process, providing the opportunity for intermixing of the PbS QDs during the growth of HP film in a facile manner.

We selected MAPI and CsPI to serve as capping ligands of our PbS QDs for their implementation in PSCs since it was

previously demonstrated that these capping ligands result in a high PCE in QD solar cells.[42,43] Furthermore, 4-aminobenzoic acid (ABA) was chosen as a PbS QD capping agent as the benzoic acid group was shown to passivate the TiO_2 electron transport layer in PSCs, resulting in a more efficient electron extraction.[47] The PbS QD ligand exchange was done in solution, as described in the Experimental section. Briefly, the as-synthesized PbS QDs with the OA ligand were dispersed in octane and the exchange ligands were separately dissolved in DMF. A phase separation was obtained after mixing the QD and ligand solutions, with the dark phase (PbS_OA in octane) on top and the ligand in DMF at the bottom. After stirring/shaking the mixed solution, phase transfer took place, and PbS QDs were transferred to the bottom phase (see Fig. S2† and the Experimental section for further details). Following ligand exchange with all of these three ligands, PbS QDs presented a redshift in PL. For MAPI and CsPI ligands, the redshift is probably due to a reduction of the degree of quantum confinement due to the ligand shell (see Fig. S3 and Section 3 of the ESI†). For ABA, the redshift could result from aggregation of QDs (see Fig. S4 and Section 3 of the ESI†). Interestingly, in the presence of MAPI precursors, there was a change in the PL spectra, suggesting the interaction of CsPI and ABA ligands with MAPI precursors (see Fig. S3 and S4 and Section 3 of the ESI†). The Fourier-transform infrared measurement of the ABA based samples also pointed towards a similar conclusion (see Fig. S5 and Section 3 of the ESI†).

The introduction of small quantities of PbS QDs with different capping ligands clearly affects the properties of the HP films. The grain sizes of HP increased slightly when PbS was introduced. Fig. 1 presents the histogram of HP grain size of HP film without and with PbS QDs with different capping ligands, determined from SEM images at several places on the films. Fig. S6† presents the top view SEM images of HP films without and with embedded PbS QDs (50 μg ml^{-1}). The dispersion of the grain size of pure MAPI film (HP, mean of 251 nm) is similar when PbS_CsPI was embedded. The average grain size increased slightly to 269 nm when PbS_MAPI was introduced and reached 283 nm (~14% increase) after the incorporation of PbS_ABA (see Fig S7† for the grain size estimation).

The X-ray diffraction (XRD) spectra of HP and hybrid HP–PbS are shown in Fig. 2a and S8.† The tetragonal structural phase, with the (110) preferential orientation corresponding to the diffraction peak at 14.2°, was obtained for all samples. The net area of diffraction peaks increased, demonstrating an increase in crystallinity when PbS QDs were introduced (see Table 1). It is worth noting that the increase in crystallinity was obtained not only for the (110) crystalline plane with the diffraction peak at 14.2° but also for the (220) crystalline plane with the diffraction peak at 28.5°. The improvement in crystallinity is, nevertheless, dependent on the capping ligand of PbS QDs despite the similar QD concentration (50 μg ml^{-1}) used for all HP + PbS samples (see Table 1). In addition, when PbS QDs were introduced in the film, the HP precursors converted more efficiently to HP, confirmed by the smaller XRD intensity of the PbI_2 diffraction peak at 12.7° (see Fig. 2b). Eventually, the analysis of the XRD spectra also indicates an increase of the (110) preferential orientation after PbS QD addition, as indicated by the increase of the ratio of the intensity of this diffraction peak with respect to other peaks (see Fig. 2a).[48]

In addition to the improvement in the structural properties, the optical properties of the HP films were also improved by the incorporation of PbS QDs. As shown in Fig. 2c, the

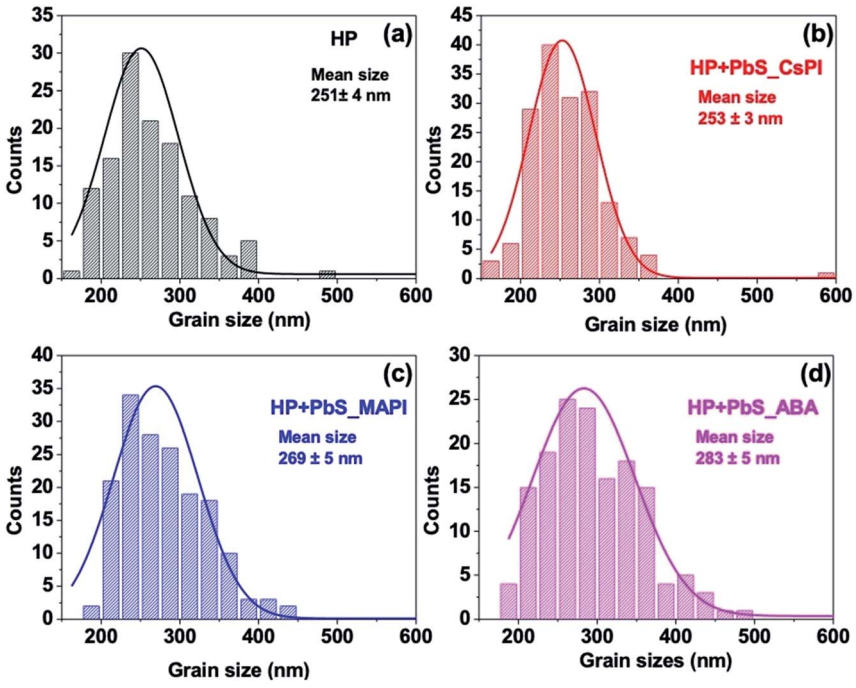

Fig. 1 Grain sizes of perovskite estimated from SEM images of (a) perovskite films without (HP) and with PbS QDs (50 μg ml^{-1}) deposited on glass of PbS QDs with the different capping ligands including (b) MAPI, (c) CsPbI and (d) 4-aminobenzoic acid (ABA).

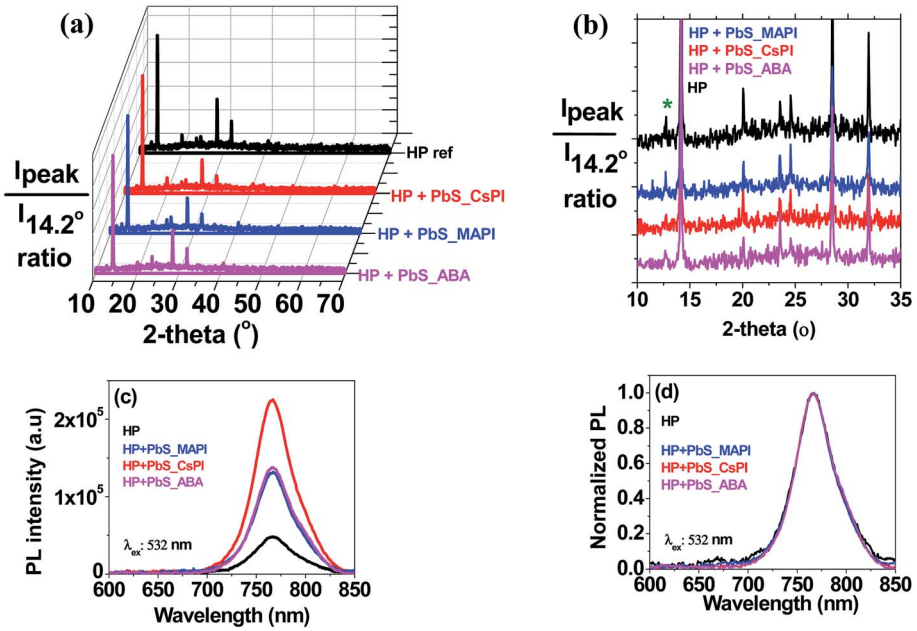

Fig. 2 Crystallographic and optical characterization of perovskite films without (HP) and with PbS QDs (50 μg ml^{-1}) deposited on glass of PbS QDs with the different capping ligands including MAPI, CsPI and 4-aminobenzoic acid (ABA). XRD spectra (a) and a zoom-in from 10 to 35° (b) (the * symbol indicates the PbI_2 diffraction peak); (c) photoluminescence (PL) and (d) normalized PL spectra.

Table 1 Net area of XRD diffraction peaks and the net area difference with respect to the HP reference sample

		HP + PbS		
2-Theta	HP	PbS_MAPI	PbS_CsPI	PbS_ABA
Net peak area (counts × 2-theta)				
14.2	9.49	11.29	11.51	11.18
28.5	3.95	4.46	4.1	5.37
32	2.89	1.98	2.58	2.25
Net area change with respect to HP				
14.2		1.8	2.02	1.69
28.5		0.51	0.15	1.42

photoluminescence (PL) intensity of HP films with PbS_ABA or PbS_MAPI was doubled with respect to the reference film, and it was tripled with PbS_CsPI QDs. This increase suggests that the intermixing of PbS QDs during the HP growth can reduce non-radiative recombination. In addition, the incorporation of a small quantity of PbS QDs did not induce any change in the optical gap of HP as no shift of PL peak position was observed for any of the hybrid films (see Fig. 2d). It is important to note that the increase in the PL was not due to the increase in the film thickness as all samples presented a similar thickness of ~ 330 nm (see Fig. S9†).

The improved morphological, structural and optical properties of the hybrid HP–PbS films can be attributed to the QDs serving as nucleation sites, which assist the crystalline growth of perovskites along the preferred orientation with bigger grain sizes as has been pointed out in previous studies.[34–36] Additionally, we also detected the dependence of HP formation on the capping ligands of embedded PbS QDs at the same concentration. Distinctly bigger perovskite grain size was obtained for ABA capping (see Fig. 1), while the highest improvement in the photoluminescence and in the structural properties, in terms of preferential orientation and crystallinity, was achieved with the use of the CsPI ligand. Additionally, the incorporation of PbS resulted in a better HP conversion from precursors with respect to the reference film, without QDs. However, the extent of HP conversion efficiency was also dependent on the capping ligands of PbS, with higher conversion for CsPI and ABA ligands (see Fig. 2b). The origin of the dependence of hybrid HP–PbS film quality on the PbS ligands is still unclear, and additional experiments would be needed to reveal the exact role of QD ligands in the formation of the hybrid films.

Finally, we also tested the potential application of the hybrid HP–PbS QD films in full solar cell devices. We selected a planar configuration, even though an improvement in PCE of HP solar cells by the incorporation of PbS QDs has been obtained in past experiments with a TiO_2 electron transport layer (ETL). The planar configuration was chosen since the alternative low temperature process SnO_2 layer[21,49] could reduce the fabrication cost and environmental impacts for future application of QDs in low-cost or large-area photovoltaics.[34–36,44] Therefore, planar solar cells were fabricated following the structure FTO/SnO_2/HP or HP–PbS/spiro-OMeTAD/Au. Fig. 3 and Table 2 present the statistical analysis of photovoltaic parameters of the fabricated devices.

Both the mean PCE of the PSCs and that of the champion cells were increased for all three capping ligands and for the two

studied concentrations, except for the case of 50 μg ml^{-1} PbS_CsPI, where no significant enhancement was observed. Fig. 4 presents the photocurrent–voltage curves of the best reference and the best hybrid solar cells. A performance improvement was achieved in all three photovoltaic parameters: open circuit voltage (V_{oc}), short circuit current density (J_{sc}) and fill factor (FF). However, the main improvement was related to the increase in FF. The improvement in performance also depends on the type of ligand for the same QD concentration. In the case of the CsPI ligand, the addition of PbS QDs slightly reduced the J_{sc} from 19.8 to 19.6 mA cm^{-2}; however, the V_{oc} and FF were enhanced, resulting in an equal or increased PCE for the PbS concentrations of 50 and 100 μg ml^{-1}, respectively, while in the case of the two other ligands, MAPI and ABA, better device performance was obtained for both PbS QD concentrations. Among the different capping ligands used, ABA showed the highest improvement with an average PCE of 15.3% for a concentration of 50 μg ml^{-1}, an improvement of over 10% with respect to the reference cells (average PCE of 13.8%). A similar improvement was observed for the champion cell, with a PCE of 16.6% (see Fig. 4). The amelioration in solar cell performance obtained for the devices based on the hybrid HP–PbS absorbers resulted from the improvement in the film quality including morphological, optical and structural properties.

A detailed analysis of the concentration effects suggests a decrease of performance for the higher concentration in the case of PbS_MAPI and PbS_ABA. The decrease of V_{oc} also observed for the higher concentrations of MAPI and ABA capping ligands points to an increase of carrier recombination with the increase of QD concentration, as was previously observed.[50] Optimization of the QD concentration is crucial since the addition of PbS QDs also introduces recombination centers and consequently the beneficial effect induced during the perovskite crystalline growth has to be properly balanced by the detrimental effect of an enhanced recombination.

The dependence of V_{oc} on the incident light intensity of planar solar cells without and with PbS_ABA QDs is shown in Fig. 5. As expected, for both cells the V_{oc} increased linearly with the increase of the incident light intensity. An ideality factor, n, can be determined from the slope of this linear relation using the equation[51]

$$n = \frac{q}{kT}\frac{dV_{oc}}{d\ln \phi}$$

where q, k, T and ϕ are the elementary charge, Boltzmann's constant, absolute temperature and light intensity, respectively. The value of the ideality factor provides important clues about the recombination process in perovskite solar cells.[52] The calculated ideality of the reference cell was close to 2 (2.18), similar to reported ideality values for other MAPI perovskite based samples.[53] This value of ideality factor points to a recombination mechanism through a Shockley–Read–Hall (SRH) recombination.[52,54] When PbS_ABA was added to the HP film, the ideality factor was reduced to 1.56, revealing lower SRH bulk recombination, for which an ideality factor of 2 is expected, and a higher relative weight of surface recombination, for which an ideality factor of 1 is expected, pointing to a decrease of trap states in the bulk HP–PbS_ABA film. This

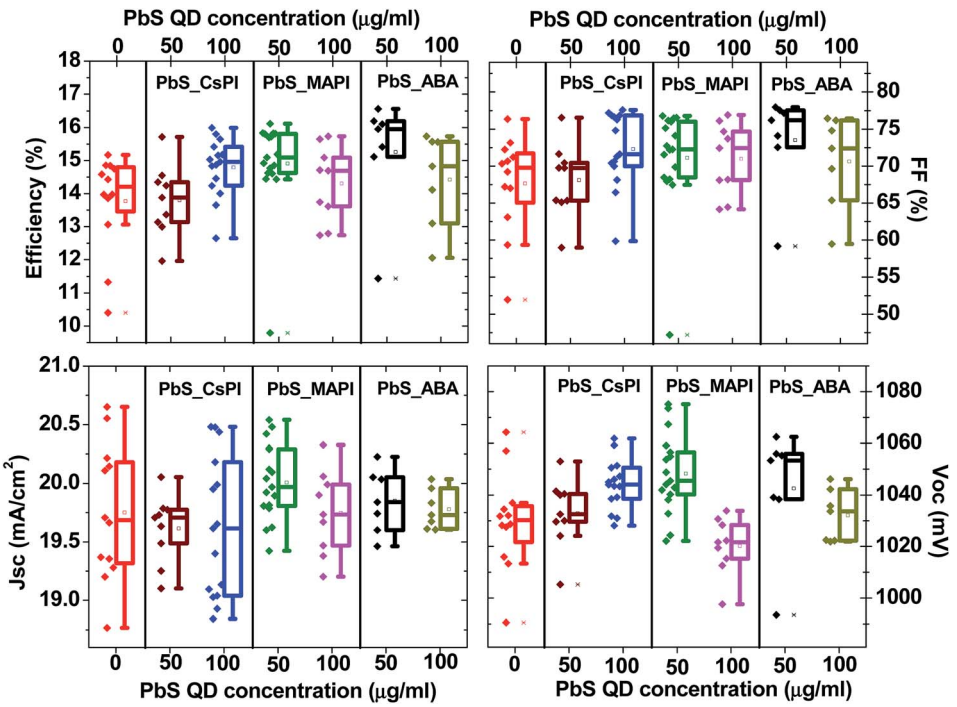

Fig. 3 Photovoltaic parameters of FTO/SnO_2/absorber/spiro-OMeTAD/Au solar cells. The different absorber layers were perovskite films without and with different PbS QD concentrations and different PbS capping ligands, including CsPI, MAPI and 4-aminobenzoic acid (ABA) separately.

Table 2 Photovoltaic parameters of the FTO/SnO_2/absorber/spiro-OMeTAD/Au solar cells presented in Fig. 3

C_{PbS} [μg ml^{-1}]	PbS ligand	J_{sc} [mA cm^{-2}]	V_{oc} [mV]	FF [%]	Efficiency [%]
0 Champion	—	19.8 ± 0.2	1030.1 ± 5.5	67.6 ± 1.9	13.8 ± 0.4
	—	19.2	1034.5	76.4	15.2
50 Champion	CsPI	19.6 ± 0.1	1032.9 ± 4.5	68.1 ± 1.7	13.8 ± 0.4
		19.5	1053.0	76.6	15.7
100 Champion		19.6 ± 0.2	1044 ± 2.5	72.3 ± 1.3	14.8 ± 0.2
		19.6	1050.6	77.6	16.0
50 Champion	MAPI	20.0 ± 0.1	1048.3 ± 3.7	71.1 ± 1.7	14.9 ± 0.3
		20.5	1044.1	75.1	16.1
100 Champion		19.7 ± 0.1	1020.2 ± 3.7	71 ± 1.6	14.3 ± 0.4
		20.0	1033.9	76.1	15.7
50 Champion	ABA	19.9 ± 0.1	1042.6 ± 8.9	73.5 ± 2.5	15.3 ± 0.7
		20.2	1055.9	77.5	16.6
100 Champion		19.8 ± 0.1	1032.1 ± 3.8	70.6 ± 2.4	14.4 ± 0.5
		19.7	1046.2	76.4	15.7

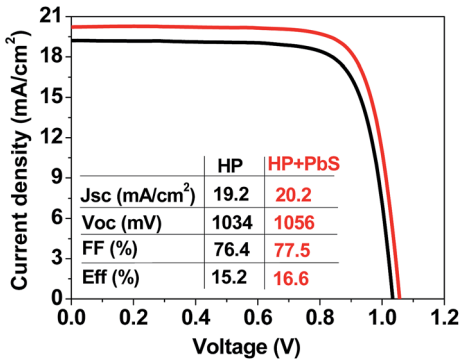

Fig. 4 Photovoltaic characteristics of the best FTO/SnO_2/absorber/spiro-OMeTAD/Au solar cells, in which absorber layers were perovskite films without (HP) and with PbS QDs (50 μg ml^{-1}) and PbS QDs had the 4-aminobenzoic acid (ABA) ligand.

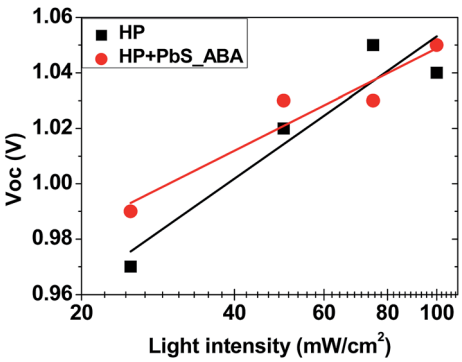

Fig. 5 Dependence of open circuit voltage on light intensity for the champion cells (see Table 2) with the architecture FTO/SnO_2/absorber/spiro-OMeTAD/Au, in which absorber layers were perovskite films without (HP) and with PbS QDs (50 μg ml^{-1}) and PbS QDs had the 4-aminobenzoic acid (ABA) ligand. The measurement was done at room temperature.

result is in agreement with an increase in the PL intensity (Fig. 2c) and an increase in V_{oc} (Fig. 3 and Table 2) when PbS QDs are incorporated.

The incident photon to current efficiency (IPCE) of solar cells based on HP without and with PbS_ABA is presented in the Fig. S10.† A similar shape of the IPCE curves was found for both cells. The incident photons were converted efficiently to current in the spectral region of 350 nm to 800 nm. The onset of photocurrent at ~800 nm was consistent with the bandgap of MAPI HP and no significant contribution to photocurrent from PbS was observed.

4. Conclusions

We show herein a detailed study of the effect of QD capping ligands on the quality of halide perovskite films obtained through intermixing of a small quantity of PbS QDs during the film crystallization. PbS QDs with three different capping ligands including MAPI, CsPI and ABA were analyzed. These QDs were added into the precursor solution of HP and hybrid HP–PbS films were prepared *via* a one-step spin-coating method. Systematic characterization shows that the presence of PbS QDs increases the grain sizes and decreases the non-radiative recombination of MAPI perovskite. Their presence also increases the preferential orientation along the (110) plane direction and crystallinity of the (110) and (220) HP crystalline planes. Consequently, improvements in the morphological, crystalline and optical properties of HP were obtained. We attribute these improvements to PbS QDs acting as nucleation sites helping in the crystallization process. As a result of the improved perovskite film quality, the performance of planar solar cells fabricated *via* low temperature processes, with SnO_2 as the ETL, was enhanced with respect to the reference cells without PbS QDs. In addition, we also observed the dependence of HP film properties on different PbS capping ligands. The ABA ligand has a higher impact on the morphological properties, while the CsPI ligand has a higher impact on the optical and structural properties. This observation could point to an improved interaction of the perovskite with the organic ligand, ABA, affecting the morphology, while the CsPI ligand likely produces a better electronic passivation at the perovskite–QD interface. The improvement in PECs of HP–PbS based solar cells

highlights the importance of PbS QD additives for the development of perovskite optoelectronic devices, an established way to improve the performance through control of the surface properties of QDs using different capping agents.

Conflicts of interest

The authors declare no competing financial interest.

Acknowledgements

This work was partially supported by the European Research Council (ERC) *via* a Consolidator Grant (724424 - No-LIMIT) and Generalitat Valenciana *via* Prometeo Grant Q-Devices (Prometeo/2018/098). We acknowledge SCIC from Jaume I University (UJI) for the help with XRD, SEM and FT-IR characterization. We thank Dr Beatriz Julián López for the absorbance measurement of PbS_OA QDs in solution. Thi Tuyen Ngo thanks the Spanish MINECO for supporting her 3 month research stay at the Weizmann Institute of Science, Israel and for her doctoral scholarships.

References

1 NREL photovoltaic efficiency chart, https://www.nrel.gov/pv/cell-efficiency.html.
2 M. M. Lee, J. Teuscher, T. Miyasaka, T. N. Murakami and H. J. Snaith, Efficient Hybrid Solar Cells Based on Meso-Superstructured Organometal Halide Perovskites, *Science*, 2012, **338**(6107), 643–647.
3 H.-S. Kim, C.-R. Lee, J.-H. Im, K.-B. Lee, T. Moehl, A. Marchioro, S.-J. Moon, R. Humphry-Baker, J.-H. Yum, J. E. Moser, M. Gratzel and N.-G. Park, Lead Iodide Perovskite Sensitized All-Solid-State Submicron Thin Film Mesoscopic Solar Cell with Efficiency Exceeding 9%, *Sci. Rep.*, 2012, **2**, 591.
4 S. D. Stranks, G. E. Eperon, G. Grancini, C. Menelaou, M. J. P. Alcocer, T. Leijtens, L. M. Herz, A. Petrozza and H. J. Snaith, Electron-Hole Diffusion Lengths Exceeding 1 Micrometer in an Organometal Trihalide Perovskite Absorber, *Science*, 2013, **342**(6156), 341–344.
5 G. Xing, N. Mathews, S. Sun, S. S. Lim, Y. M. Lam, M. Grätzel, S. Mhaisalkar and T. C. Sum, Long-Range Balanced Electron- and Hole-Transport Lengths in Organic–Inorganic $CH_3NH_3PbI_3$, *Science*, 2013, **342**(6156), 344–347.
6 O. A. Jaramillo-Quintero, R. S. Sanchez, M. Rincon and I. Mora-Sero, Bright Visible-Infrared Light Emitting Diodes Based on Hybrid Halide Perovskite with Spiro-OMeTAD as a Hole-Injecting Layer, *J. Phys. Chem. Lett.*, 2015, **6**(10), 1883–1890.
7 Z.-K. Tan, R. S. Moghaddam, M. L. Lai, P. Docampo, R. Higler, F. Deschler, M. Price, A. Sadhanala, L. M. Pazos, D. Credgington, F. Hanusch, T. Bein, H. J. Snaith and R. H. Friend, Bright light-emitting diodes based on organometal halide perovskite, *Nat. Nanotechnol.*, 2014, **9**(9), 687–692.
8 K. Lin, J. Xing, L. N. Quan, F. P. G. de Arquer, X. Gong, J. Lu, L. Xie, W. Zhao, D. Zhang, C. Yan, W. Li, X. Liu, Y. Lu, J. Kirman, E. H. Sargent, Q. Xiong and Z. Wei, Perovskite light-emitting diodes with external quantum efficiency exceeding 20 per cent, *Nature*, 2018, **562**(7726), 245–248.
9 L. Dou, Y. Yang, J. You, Z. Hong, W.-H. Chang and G. Li, Solution-processed hybrid perovskite photodetectors with high detectivity, *Nat. Commun.*, 2014, **5**, 5404.
10 I. Suárez, E. J. Juárez-Pérez, J. Bisquert, I. Mora-Seró and J. P. Martínez-Pastor, Polymer/Perovskite Amplifying Waveguides for Active Hybrid Silicon Photonics, *Adv. Mater.*, 2015, **27**(40), 6157–6162.
11 I. Suárez, E. Hassanabadi, A. Maulu, N. Carlino, C. A. Maestri, M. Latifi, P. Bettotti, I. Mora-Seró and J. P. Martínez-Pastor, Integrated Optical Amplifier–Photodetector on a Wearable Nanocellulose Substrate, *Adv. Opt. Mater.*, 2018, **6**(12), 1800201.
12 F. Deschler, M. Price, S. Pathak, L. E. Klintberg, D.-D. Jarausch, R. Higler, S. Hüttner, T. Leijtens, S. D. Stranks, H. J. Snaith, M. Atatüre, R. T. Phillips and R. H. Friend, High Photoluminescence Efficiency and Optically Pumped Lasing in Solution-Processed Mixed Halide Perovskite Semiconductors, *J. Phys. Chem. Lett.*, 2014, **5**(8), 1421–1426.
13 H. Zhu, Y. Fu, F. Meng, X. Wu, Z. Gong, Q. Ding, M. V. Gustafsson, M. T. Trinh, S. Jin and X. Y. Zhu, Lead halide perovskite nanowire lasers with low lasing thresholds and high quality factors, *Nat. Mater.*, 2015, **14**(6), 636–642.
14 G. Xing, N. Mathews, S. S. Lim, N. Yantara, X. Liu, D. Sabba, M. Grätzel, S. Mhaisalkar and T. C. Sum, Low-temperature solution-processed wavelength-tunable perovskites for lasing, *Nat. Mater.*, 2014, **13**(5), 476–480.
15 M. Saliba, J.-P. Correa-Baena, C. M. Wolff, M. Stolterfoht, N. Phung, S. Albrecht, D. Neher and A. Abate, How to Make over 20% Efficient Perovskite Solar Cells in Regular (n–i–p) and Inverted (p–i–n) Architectures, *Chem. Mater.*, 2018, **30**(13), 4193–4201.
16 L.-J. Chen, C.-R. Lee, Y.-J. Chuang, Z.-H. Wu and C. Chen, Synthesis and Optical Properties of Lead-Free Cesium Tin Halide Perovskite Quantum Rods with High-Performance Solar Cell Application, *J. Phys. Chem. Lett.*, 2016, **7**(24), 5028–5035.
17 N. J. Jeon, J. H. Noh, Y. C. Kim, W. S. Yang, S. Ryu and S. I. Seok, Solvent engineering for high-performance inorganic–organic hybrid perovskite solar cells, *Nat. Mater.*, 2014, **13**(9), 897–903.
18 M. Saliba, T. Matsui, K. Domanski, J.-Y. Seo, A. Ummadisingu, S. M. Zakeeruddin, J.-P. Correa-Baena, W. R. Tress, A. Abate, A. Hagfeldt and M. Grätzel, Incorporation of rubidium cations into perovskite solar cells improves photovoltaic performance, *Science*, 2016, **354**(6309), 206–209.
19 W. Zhang, M. Anaya, G. Lozano, M. E. Calvo, M. B. Johnston, H. Míguez and H. J. Snaith, Highly Efficient Perovskite Solar Cells with Tunable Structural Color, *Nano Lett.*, 2015, **15**(3), 1698–1702.

20 H. Zhou, Q. Chen, G. Li, S. Luo, T.-b. Song, H.-S. Duan, Z. Hong, J. You, Y. Liu and Y. Yang, Interface engineering of highly efficient perovskite solar cells, *Science*, 2014, **345**(6196), 542–546.

21 J. P. Correa Baena, L. Steier, W. Tress, M. Saliba, S. Neutzner, T. Matsui, F. Giordano, T. J. Jacobsson, A. R. Srimath Kandada, S. M. Zakeeruddin, A. Petrozza, A. Abate, M. K. Nazeeruddin, M. Gratzel and A. Hagfeldt, Highly efficient planar perovskite solar cells through band alignment engineering, *Energy Environ. Sci.*, 2015, **8**(10), 2928–2934.

22 S. Masi, F. Aiello, A. Listorti, F. Balzano, D. Altamura, C. Giannini, R. Caliandro, G. Uccello-Barretta, A. Rizzo and S. Colella, Connecting the solution chemistry of PbI_2 and MAI: a cyclodextrin-based supramolecular approach to the formation of hybrid halide perovskites, *Chem. Sci.*, 2018, **9**(12), 3200–3208.

23 J. Xu, A. Buin, A. H. Ip, W. Li, O. Voznyy, R. Comin, M. Yuan, S. Jeon, Z. Ning, J. J. McDowell, P. Kanjanaboos, J.-P. Sun, X. Lan, L. N. Quan, D. H. Kim, I. G. Hill, P. Maksymovych and E. H. Sargent, Perovskite–fullerene hybrid materials suppress hysteresis in planar diodes, *Nat. Commun.*, 2015, **6**, 7081.

24 T. T. Ngo, I. Suarez, G. Antonicelli, D. Cortizo-Lacalle, J. P. Martinez-Pastor, A. Mateo-Alonso and I. Mora-Sero, Enhancement of the Performance of Perovskite Solar Cells, LEDs, and Optical Amplifiers by Anti-Solvent Additive Deposition, *Adv. Mater.*, 2017, **29**, 1604056.

25 A. Fakharuddin, M. Seybold, A. Agresti, S. Pescetelli, F. Matteocci, M. I. Haider, S. T. Birkhold, H. Hu, R. Giridharagopal, M. Sultan, I. Mora-Seró, A. Di Carlo and L. Schmidt-Mende, Perovskite-Polymer Blends Influencing Microstructures, Nonradiative Recombination Pathways, and Photovoltaic Performance of Perovskite Solar Cells, *ACS Appl. Mater. Interfaces*, 2018, **10**(49), 42542–42551.

26 A. Giuri, S. Masi, A. Listorti, G. Gigli, S. Colella, C. E. Corcione and A. Rizzo, Polymeric rheology modifier allows single-step coating of perovskite ink for highly efficient and stable solar cells, *Nano Energy*, 2018, **54**, 400–408.

27 B. Chaudhary, A. Kulkarni, A. K. Jena, M. Ikegami, Y. Udagawa, H. Kunugita, K. Ema and T. Miyasaka, Poly(4-Vinylpyridine)-Based Interfacial Passivation to Enhance Voltage and Moisture Stability of Lead Halide Perovskite Solar Cells, *ChemSusChem*, 2017, **10**(11), 2473–2479.

28 X. Li, M. Ibrahim Dar, C. Yi, J. Luo, M. Tschumi, S. M. Zakeeruddin, M. K. Nazeeruddin, H. Han and M. Grätzel, Improved performance and stability of perovskite solar cells by crystal crosslinking with alkylphosphonic acid ω-ammonium chlorides, *Nat. Chem.*, 2015, **7**, 703.

29 L. Zuo, H. Guo, D. W. deQuilettes, S. Jariwala, N. De Marco, S. Dong, R. DeBlock, D. S. Ginger, B. Dunn, M. Wang and Y. Yang, Polymer-modified halide perovskite films for efficient and stable planar heterojunction solar cells, *Sci. Adv.*, 2017, **3**(8), e1700106.

30 T. T. Ngo, I. Suarez, R. S. Sanchez, J. P. Martinez-Pastor and I. Mora-Sero, Single step deposition of an interacting layer of a perovskite matrix with embedded quantum dots, *Nanoscale*, 2016, **8**, 14379–14383.

31 Z. Ning, X. Gong, R. Comin, G. Walters, F. Fan, O. Voznyy, E. Yassitepe, A. Buin, S. Hoogland and E. H. Sargent, Quantum-dot-in-perovskite solids, *Nature*, 2015, **523**(7560), 324–328.

32 T. T. Ngo and I. Mora-Seró, Interaction between Colloidal Quantum Dots and Halide Perovskites: Looking for Constructive Synergies, *J. Phys. Chem. Lett.*, 2019, **10**(5), 1099–1108.

33 M. Liu, Y. Chen, C.-S. Tan, R. Quintero-Bermudez, A. H. Proppe, R. Munir, H. Tan, O. Voznyy, B. Scheffel, G. Walters, A. P. T. Kam, B. Sun, M.-J. Choi, S. Hoogland, A. Amassian, S. O. Kelley, F. P. García de Arquer and E. H. Sargent, Lattice anchoring stabilizes solution-processed semiconductors, *Nature*, 2019, **570**(7759), 96–101.

34 J. Han, S. Luo, X. Yin, Y. Zhou, H. Nan, J. Li, X. Li, D. Oron, H. Shen and H. Lin, Hybrid PbS Quantum-Dot-in-Perovskite for High-Efficiency Perovskite Solar Cell, *Small*, 2018, **14**(31), 1801016.

35 S.-S. Li, C.-H. Chang, Y.-C. Wang, C.-W. Lin, D.-Y. Wang, J.-C. Lin, C.-C. Chen, H.-S. Sheu, H.-C. Chia, W.-R. Wu, U. S. Jeng, C.-T. Liang, R. Sankar, F.-C. Chou and C.-W. Chen, Intermixing-seeded growth for high-performance planar heterojunction perovskite solar cells assisted by precursor-capped nanoparticles, *Energy Environ. Sci.*, 2016, **9**(4), 1282–1289.

36 J. Han, X. Yin, H. Nan, Y. Zhou, Z. Yao, J. Li, D. Oron and H. Lin, Enhancing the Performance of Perovskite Solar Cells by Hybridizing SnS Quantum Dots with $CH_3NH_3PbI_3$, *Small*, 2017, **13**(32), 1700953.

37 M. S. de la Fuente, R. S. Sánchez, V. González-Pedro, P. P. Boix, S. G. Mhaisalkar, M. E. Rincón, J. Bisquert and I. Mora-Seró, Effect of Organic and Inorganic Passivation in Quantum-Dot-Sensitized Solar Cells, *J. Phys. Chem. Lett.*, 2013, **4**(9), 1519–1525.

38 A. H. Ip, S. M. Thon, S. Hoogland, O. Voznyy, D. Zhitomirsky, R. Debnath, L. Levina, L. R. Rollny, G. H. Carey, A. Fischer, K. W. Kemp, I. J. Kramer, Z. Ning, A. J. Labelle, K. W. Chou, A. Amassian and E. H. Sargent, Hybrid passivated colloidal quantum dot solids, *Nat. Nanotechnol.*, 2012, **7**(9), 577–582.

39 Y. Yang, B. Zhao, Y. Gao, H. Liu, Y. Tian, D. Qin, H. Wu, W. Huang and L. Hou, Novel Hybrid Ligands for Passivating PbS Colloidal Quantum Dots to Enhance the Performance of Solar Cells, *Nano-Micro Lett.*, 2015, **7**(4), 325–331.

40 Z. Ning, H. Dong, Q. Zhang, O. Voznyy and E. H. Sargent, Solar Cells Based on Inks of n-Type Colloidal Quantum Dots, *ACS Nano*, 2014, **8**(10), 10321–10327.

41 M. Liu, O. Voznyy, R. Sabatini, F. P. Garcia de Arquer, R. Munir, A. H. Balawi, X. Lan, F. Fan, G. Walters, A. R. Kirmani, S. Hoogland, F. Laquai, A. Amassian and E. H. Sargent, Hybrid organic–inorganic inks flatten the

energy landscape in colloidal quantum dot solids, *Nat. Mater.*, 2017, **16**(2), 258–263.

42 Z. Yang, A. Janmohamed, X. Lan, F. P. García de Arquer, O. Voznyy, E. Yassitepe, G.-H. Kim, Z. Ning, X. Gong, R. Comin and E. H. Sargent, Colloidal Quantum Dot Photovoltaics Enhanced by Perovskite Shelling, *Nano Lett.*, 2015, **15**(11), 7539–7543.

43 X. Zhang, J. Zhang, D. Phuyal, J. Du, L. Tian, V. A. Öberg, M. B. Johansson, U. B. Cappel, O. Karis, J. Liu, H. Rensmo, G. Boschloo and E. M. J. Johansson, Inorganic $CsPbI_3$ Perovskite Coating on PbS Quantum Dot for Highly Efficient and Stable Infrared Light Converting Solar Cells, *Adv. Energy Mater.*, 2018, **8**(6), 1702049.

44 J.-A. Alberola-Borràs, R. Vidal, E. J. Juárez-Pérez, E. Mas-Marzá, A. Guerrero and I. Mora-Seró, Relative impacts of methylammonium lead triiodide perovskite solar cells based on life cycle assessment, *Sol. Energy Mater. Sol. Cells*, 2018, **179**, 169–177.

45 I. Moreels, K. Lambert, D. Smeets, D. De Muynck, T. Nollet, J. C. Martins, F. Vanhaecke, A. Vantomme, C. Delerue, G. Allan and Z. Hens, Size-Dependent Optical Properties of Colloidal PbS Quantum Dots, *ACS Nano*, 2009, **3**(10), 3023–3030.

46 D. Yang, R. Yang, K. Wang, C. Wu, X. Zhu, J. Feng, X. Ren, G. Fang, S. Priya and S. Liu, High efficiency planar-type perovskite solar cells with negligible hysteresis using EDTA-complexed SnO_2, *Nat. Commun.*, 2018, **9**(1), 3239.

47 K. Wojciechowski, S. D. Stranks, A. Abate, G. Sadoughi, A. Sadhanala, N. Kopidakis, G. Rumbles, C.-Z. Li, R. H. Friend, A. K. Y. Jen and H. J. Snaith, Heterojunction Modification for Highly Efficient Organic–Inorganic Perovskite Solar Cells, *ACS Nano*, 2014, **8**(12), 12701–12709.

48 S. Yen-Chen, L. Yu-Bing, L. Chia-Shuo, H. Hsiao-Chi, W. Leeyih, W. Chih-I and L. King-Fu, Amino-Acid-Induced Preferential Orientation of Perovskite Crystals for Enhancing Interfacial Charge Transfer and Photovoltaic Performance, *Small*, 2017, **13**(22), 1604305.

49 Q. Jiang, L. Zhang, H. Wang, X. Yang, J. Meng, H. Liu, Z. Yin, J. Wu, X. Zhang and J. You, Enhanced electron extraction using SnO_2 for high-efficiency planar-structure $HC(NH_2)_2PbI_3$-based perovskite solar cells, *Nat. Energy*, 2016, **2**, 16177.

50 P. Galar, P. Piatkowski, T. T. Ngo, M. Gutiérrez, I. Mora-Seró and A. Douhal, Perovskite-quantum dots interface: Deciphering its ultrafast charge carrier dynamics, *Nano Energy*, 2018, **49**, 471–480.

51 T. Kirchartz, F. Deledalle, P. S. Tuladhar, J. R. Durrant and J. Nelson, On the Differences between Dark and Light Ideality Factor in Polymer:Fullerene Solar Cells, *J. Phys. Chem. Lett.*, 2013, **4**(14), 2371–2376.

52 W. Tress, M. Yavari, K. Domanski, P. Yadav, B. Niesen, J. P. C. Baena, A. Hagfeldt and M. Graetzel, Interpretation and evolution of open-circuit voltage, recombination, ideality factor and subgap defect states during reversible light-soaking and irreversible degradation of perovskite solar cells, *Energy Environ. Sci.*, 2018, **11**(1), 151–165.

53 O. Almora, K. T. Cho, S. Aghazada, I. Zimmermann, G. J. Matt, C. J. Brabec, M. K. Nazeeruddin and G. Garcia-Belmonte, Discerning recombination mechanisms and ideality factors through impedance analysis of high-efficiency perovskite solar cells, *Nano Energy*, 2018, **48**, 63–72.

54 W. Shockley and W. T. Read, Statistics of the Recombinations of Holes and Electrons, *Phys. Rev.*, 1952, **87**(5), 835–842.

